Journal of Functional Materials and Applied Engineering

Research Paper

Performance of Bamboo-Based Activated Carbon in Enhancing CO_2 Absorption by Aqueous Diethanolamine Solution

Alith Averseng[1], Yohann Van Zee[2,*]

[1] Department of Chemical Sciences, University of Naples Federico II, 80126 Naples, Italy
[2] Université Grenoble Alpes, Université Savoie Mont Blanc, CNRS, Grenoble INP, LEPMI, 38000 Grenoble, France
*Corresponding author: Y.VanZee@grenoble-inp.f

Abstract. The large diffusion resistance of CO_2 in aqueous diethanolamine (DEA) solution is the primary factor resulting in its slow absorption rate. By introducing a small amount of bamboo-based activated carbon (BAC), the diffusion resistance of CO_2 in 30% DEA-H_2O is significantly reduced, thereby effectively enhancing the CO_2 absorption rate. In this study, five types of BAC with different pore size distributions were prepared by adjusting the mass ratio of bamboo charcoal (BC) to the activator of potassium hydroxide (KOH). The hybrid sorbent of 30% DEA-BAC-H_2O for CO_2 absorption (adsorption) was developed. CO_2 absorption (adsorption) capacity, rate, and desorption enthalpy of the hybrid sorbent were systematically measured, calculated as well as compared with the commercial absorbents. The results showed that when the mass ratio of BC to KOH was 1:2 (denoted as BAC_1:$_2$), BAC_1:$_2$ exhibited a well-developed specific surface area and micropore volume (pore size ≤1 nm). Under this condition, the CO_2 absorption (adsorption) rate in 30% DEA-1% BAC_1:$_2$-H_2O was 7 times and 3.5 times those of 30% DEA-H_2O and 25.5% DEA-4.5% piperazine (PZ)-H_2O (a commercial absorbent), respectively. Meanwhile, CO_2 absorption (adsorption) capacity of 30% DEA-1% BAC_1:$_2$-H_2O was moderate, and the CO_2 desorption enthalpy was reduced by 25% compared with that of 25.5% DEA-4.5% PZ-H_2O, demonstrating its potential for industrial application.

Keywords: *Activated carbon; CO_2 capture; Diffusion resistance; Thermodynamics; Mass transfer*

Received on 15 April 2023, Accepted on 06 June 2023, Published on 28 July 2023

1 Introduction

The increase in atmospheric carbon dioxide (CO_2) concentration and the resulting global climate change have garnered widespread attention in recent decades. To address this challenge, reducing atmospheric CO_2 levels has become a critical issue requiring urgent solutions. Currently, CO_2 capture technologies primarily include adsorption, absorption, and membrane separation methods. Among these approaches, chemical absorption stands out as a predominant technology, attributed to its superior efficiency, pronounced selectivity, and extensive industrial applicability [1-2]. Within the broad spectrum of chemical absorbents available,diethanolamine (DEA) has garnered significant research interest owing to its economic viability, favorable reactivity profile, and reduced corrosive characteristics [3]. However, the kinetics of CO_2 capture by DEA solutions remain comparatively sluggish when benchmarked against alternative amine-based systems, resulting in more substantial equipment footprints and elevated energy demands for carbon dioxide separation processes [4]. Therefore, it is necessary to further develop efficient CO_2 capture systems based on DEA solutions to increase the CO_2 absorption rate, thereby improving CO_2 capture efficiency and reducing capture costs.

In recent years, extensive research has been conducted on enhancing the absorption kinetics and reaction mechanisms of CO_2 in DEA solutions [5-6]. For example, introducing the traditional activator piperazine (PZ) into DEA solutions can significantly accelerate the reaction kinetics between DEA and CO_2, greatly improving the CO_2 absorption rate in DEA solutions [7]. Similarly, the synergistic effect between monoethanolamine (MEA) and DEA can also increase the CO_2 absorption rate of DEA solutions [8]. However, enhancing the reaction rate by adjusting the chemical reaction between DEA and CO_2 inevitably leads to increased energy consumption during the

desorption process [9]. According to non-equilibrium thermodynamic principles [10], reducing the diffusion resistance of CO_2 in DEA solutions and increasing the gas-liquid contact area can also effectively enhance the CO_2 absorption rate [11], such as by adding solid materials [12-13]. Previous studies have shown that adding 0.01% – 0.10% (mass fraction) titanium dioxide (TiO_2) in a continuous stirred bubble column can increase the CO_2 absorption rate in DEA solutions by 25.2% – 43.8% [14]. However, traditional solid materials, such as TiO_2, aluminum oxide, and silicon dioxide, have high production costs (especially high-purity or nanoscale materials), making large-scale application difficult. Consequently, the development of economically viable, high-efficacy solid-phase materials to augment the CO_2 capture kinetics of DEA-based systems represents a critical research priority, thereby facilitating the advancement and widespread implementation of efficient carbon capture methodologies.Compared to traditional solid materials, activated carbon (AC) itself has a physical adsorption capacity for CO_2. Its surface oxygen-containing functional groups further enhance the synergistic effect with amine groups, and its pore structure can extend the residence time of CO_2 [16]. In contrast, traditional solid materials primarily promote the reaction through mass transfer enhancement, relying on the chemical reaction of amine solutions and lacking independent adsorption capacity [17]. Furthermore, AC has lower toxicity and environmental risk and is recyclable. Traditional solid materials may cause ecological problems due to release into the environment during long-term use, requiring additional safety considerations [19]. In this context, activated carbon (AC) emerges as a compelling candidate given its established manufacturing infrastructure and economic accessibility,and has found extensive utility within carbon dioxide sequestration applications. For instance, prior investigations have demonstrated that activated carbon (AC), characterized by its well-developed porous architecture and exceptional specific surface area, can attain CO_2 uptake capacities reaching 8.44 mmol/g [20]. Meanwhile, introducing AC into a solution to form a slurry system can also exhibit good CO_2 adsorption performance. It has been found that the presence of AC in hybrid systems can significantly increase the CO_2 absorption (adsorption) rate [22]. Additionally, introducing AC into the high-pressure water scrubbing process for CO_2 separation found that the CO_2 absorption (adsorption) rate in the hybrid system increased by 57% compared to the pure water system [23]. These performance improvements originate from the microporous architecture of activated carbon—particularly pores with diameters below 1.0 nm—facilitating the transport and accessibility of CO_2 molecules within the internal pore network.On the other hand, introducing AC into organic amine solutions can also significantly increase the CO_2 absorption rate. Adding AC prepared from waste walnut shells to MEA solutions can increase the CO_2 absorption (adsorption) rate by 1.5 times, with a similar enhancement mechanism to the aforementioned studies [24]. Therefore, introducing AC into DEA solutions has also become a potential strategy to enhance the CO_2 absorption rate.

Bamboo-derived activated carbon (BAC) has emerged as a material of considerable interest, attributable to its elevated specific surface area and well-developed porous characteristics, exhibiting enhanced efficacy in carbon dioxide sequestration applications [25]. Meanwhile, China has abundant bamboo resources. Bamboo, as a renewable resource with fast growth and ample reserves, holds significant value for development and utilization. Compared to coconut shell activated carbon priced between 7000–12000 CNY/t, bamboo-based activated carbon, due to advantages in raw material and processing costs, is priced at about 60% of that, making it more suitable for low-cost applications [27]. The CO_2 adsorption capacity of BAC at 273.2 K and 0.1 MPa is as high as 7.0 mmol/g, significantly higher than other carbon materials. However, BAC not only has excellent CO_2 adsorption capacity but also demonstrates a significant rate enhancement effect. For instance, a 7% mass fraction BAC aqueous solution increased the CO_2 absorption (adsorption) rate by 2.7 times compared to the pure water system [28]. Therefore, introducing BAC into DEA solutions to increase the CO_2 absorption rate holds great application potential. Moreover, BAC synthesized employing potassium hydroxide (KOH) as the chemical activating agent displays a pronounced microporous architecture, featuring pore dimensions predominantly distributed within the 0.7–1.0 nm interval.This pore size distribution shows significant adsorption advantages for CO_2 [29-30].

This study aims to enhance the CO_2 absorption rate by introducing BAC into DEA solutions. The pore structure of BAC was adjusted by controlling the BC/KOH mass ratio. A DEA-BAC-H_2O system for CO_2 absorption (adsorption) was developed. The CO_2 absorption (adsorption) rate, capacity, and desorption enthalpy of this system were systematically measured and calculated, and compared with commercial absorbents. The developed 30% DEA-1% $BAC_{1:2}$-H_2O (mass fraction, same below) shows promising potential for industrial application.

2 Materials and Methods

2.1 Materials

N_2 and CO_2 (volume fraction >99.9%), Nanjing Maxnan Special Gases Co., Ltd.; DEA (mass fraction >99.7%), Shanghai Lingfeng Chemical Reagent Co., Ltd.; KOH, Xilong Scientific Co., Ltd.; HCl, Sinopharm Chemical Reagent Co., Ltd.

Preparation of BAC: Raw bamboo specimens were procured from a commercial vendor located in Nanjing, China. The obtained material was sectioned into segments measuring approximately 2 cm in width,subsequently rinsed extensively with flowing tap water to eliminate superficial contaminants, followed by thermal treatment in a drying oven maintained at 383.2 K for a duration of 24 hours. The pretreated bamboo specimens underwent initial carbonization through a controlled pyrolytic process. A mass of approximately 200 g of the prepared bamboo material was positioned within a tubular furnace under an inert nitrogen atmosphere, heated to 873.2 K at a controlled ramp rate of 5 K/min, and maintained at this temperature for 2 hours, after which the system was allowed to cool passively to ambient temperature to retrieve the carbonized product. To augment the porous architecture and specific surface area of the carbonized product, potassium hydroxide (KOH) was employed as the chemical activating agent. Activation treatment was performed by adjusting the BC/KOH mass ratio (1:0.5, 1:1, 1:2, 1:3, and 1:4). Before activation, BC was crushed to an average particle size of 71.0 μm and dried in a blast drying oven at 423.2 K for 5 h. BC and KOH were mechanically ground in a mortar at the predetermined mass ratio until the KOH chunks were completely powdered and uniformly dispersed with the BC. The activation procedure was performed in a muffle furnace, with the temperature elevated from 308 K to 1073 K at a heating rate of 5 K/min, and subsequently held at 1073 K for a duration of 1 hour. Upon completion of the activation process, the specimen was allowed to cool passively to ambient temperature. The activated product was subsequently washed with an aqueous 1.0 mol/L HCl solution until the pH stabilized at 1. The material was then filtered and exhaustively rinsed with deionized water until the effluent attained neutral pH. Finally, the sample was preserved in a sealed desiccator under ambient conditions.

2.2 Experimental Methods

2.2.1 Measurement of CO_2 Absorption (Adsorption) Capacity and Rate

The schematic illustration of the experimental apparatus employed for quantifying CO_2 capture capacity and kinetics is presented in Figure 1, comprising primarily a gas reservoir and an equilibrium vessel equipped with magnetic agitation. Thermal control for both the gas reservoir and equilibrium chamber was achieved using a water bath system maintaining precision within ±0.1 K. Pressure tracking was accomplished through two Rosemount 2088G pressure transducers with an accuracy of ±1 kPa. During the experimental procedure, a volume of approximately 10.0 mL of the hybrid formulation was introduced into the equilibrium chamber and subjected to degassing via a vacuum pump (pressure <0.012 MPa). Following this, the initial pressure within the equilibrium vessel was allowed to equilibrate for a duration of 15 minutes. with the stabilized pressure recorded as p_o. Upon initiation of the measurement, a predetermined quantity of CO_2 was rapidly introduced into the equilibrium chamber within a 3-second interval, with concurrent activation of the magnetic stirring mechanism.maintaining a constant rotational speed of 200 r/min to preserve an undisturbed gas-liquid boundary. Throughout the initial 10-minute interval of the measurement, pressure variations within the equilibrium vessel were logged at 2-second intervals by the automated data acquisition system. To ensure data reliability, uniformity in the initial CO_2 partial pressure was preserved to the greatest extent practicable. Upon stabilization of the equilibrium cell pressure for a duration exceeding 2 hours, the CO_2 uptake by the hybrid system was deemed to have attained equilibrium. The equilibrium amount of CO_2 absorbed (adsorbed) in the hybrid system was calculated based on the change in CO_2 pressure inside the equilibrium cell before and after absorption (adsorption). Additionally, each experimental condition was conducted in triplicate, with the mean value reported as the definitive outcome.

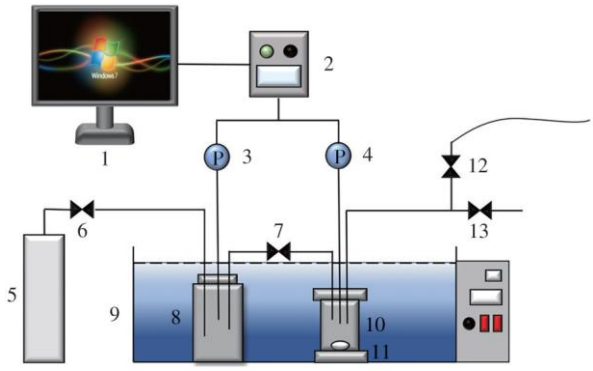

Figure 1 Experimental setup

1- Automatic data collection system; 2- Data collector; 3. 4- Pressure gauge; 5- CO2 gas cylinder; 6. 7, 12, 13- Valves; 8- Gas storage tank; 9- Water bath; 10- Balance kettle; 11- Magnetic stirrer

The molar concentration of CO_2 in the hybrid absorbent (adsorbent) was calculated using Equations (1) and (2).

$$n(CO2)=Z1RT(p1-pV)(VC-VL)-Z2RT(p2-pV)(VC-VL) \quad (1)$$

$$C(CO2)=mLn(CO2) \quad (2)$$

Where, n(CO2) is the molar amount of CO_2, mol; p1 and p2 are the initial and equilibrium CO_2 partial pressures, respectively, Pa; pV is the initial pressure in the equilibrium cell, Pa; VC and VL are the volumes of the equilibrium cell and the hybrid system, respectively, cm^3; Z1 and Z2 are the CO_2 compressibility factors at the corresponding states (calculated using the second virial coefficient); Tis the temperature in Kelvin, K; Ris the gas constant, R=8.314 J/(mol\cdotpK); mL is the mass of the hybrid system, g; C(CO2) is the molar concentration of CO_2, mol/g.

According to the Damping-Film theory, the apparent absorption (adsorption) rate constant (k) can be calculated using Equation (3) [31].

$$lnn-nen0-ne=kt \quad (3)$$

Where, nis the molar amount of CO_2 in the equilibrium cell at time t, mol; n0 and ne are the molar amounts of CO_2 at the initial time and at equilibrium, respectively, mol; kis the apparent absorption (adsorption) rate constant, s^{-1} .

It should be specifically noted that this hybrid system exhibits a multi-mechanism synergistic effect of chemical absorption by the DEA solution and physical adsorption by BAC. Within the multiphase gas-liquid-solid coupled mass transfer system, the apparent rate constant serves as a more suitable descriptor for characterizing the absorption kinetics. This parameter differs from the intrinsic rate constant k', which needs to be obtained through calculations under specific experimental conditions [32]. By systematically integrating the coupling effects of mass transfer resistance and reaction kinetics, this parameter achieves a comprehensive evaluation of the dynamic process of the multiphase reaction system. Its numerical result essentially reflects a macroscopic dynamic characteristic parameter [33].

2.2.2 Analysis of CO_2 Mass Transfer Resistance

According to non-equilibrium thermodynamic theory [10], the mass transfer resistance of CO_2 in the hybrid system (1/k) can be further decomposed into diffusion resistance (1/kd) and reaction resistance (1/ks), as shown in Equation (4).

$$1=kd1+ks1 \quad (4)$$

2.2.3 Calculation of CO_2 Desorption Enthalpy

The CO_2 desorption enthalpy (Δ H) is an important indicator for measuring the regeneration energy consumption of the hybrid system. Its value can be obtained from the Gibbs-Helmholtz equation, as shown in Equation (5)

[34].

$$\Delta H = -RT2\partial T\partial \ln p \quad (5)$$

Where, pis the equilibrium partial pressure of CO_2 at a specific absorption (adsorption) capacity, kPa; ΔHis the desorption enthalpy, kJ/mol.

2.2.4 Cycling Experiments of the Hybrid System

As shown in Figure 2, regeneration experiments were conducted using a three-necked flask in an oil bath. The system pressure was set to atmospheric pressure, the temperature was maintained at 373.2 K, and the experiment lasted for 60 minutes. Furthermore, to maintain a constant H_2O concentration in the hybrid absorbent (adsorbent), an appropriate amount of H_2O was replenished during the regeneration process to ensure the stability of the system in subsequent CO_2 absorption (adsorption) experiments.

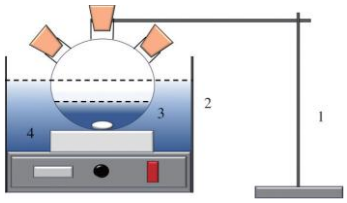

Figure 2 Figure 2 Loop Experiment Device

1- Bracket; 2- Oil bath pot; 3-Three necked flask; 4- Magnetic stirrer

2.3 Characterization and Testing

The pore size distribution of BAC was determined employing a fully automated surface area and porosity analyzer (ASAP 2460, Micromeritics, USA). The specific surface area of BAC was determined via the Brunauer-Emmet-Teller (BET) method. while the pore structural parameters were derived using Non-Local Density Functional Theory (NLDFT). The surface morphological characteristics of the specimens were examined utilizing a field-emission scanning electron microscope (SEM, Zeiss Gemini Sigma 300 VP). The thermal stability profiles of the specimens were evaluated employing a thermogravimetric analyzer (STA 8000).

3 Results and Discussion

3.1 Characterization Analysis

3.1.1 Surface Morphology of BAC

Figure 3 shows SEM images of five BAC samples with different KOH activation ratios, with BC as the control group. The results show that as the KOH mass ratio increases, the corrosive effect of KOH becomes more pronounced, leading to gradually rougher surface features of the BAC. Concurrently, the surface morphology of $BAC_{1:2}$ displays more pronounced void structures, underscoring the efficacy of KOH as an activating agent throughout the thermal treatment process. Notably, at BC/KOH mass ratios exceeding 1:2, the pore volume undergoes further expansion, which facilitates the transport of CO_2 molecules into the internal pore network of BAC. Consequently, for BC/KOH mass ratios of 1:2 or greater, the conditions become particularly favorable for fabricating BAC with a well-developed porous architecture.However, when the BC/KOH mass ratio is 1:4, the micropore size on the BAC surface further increases, a phenomenon consistent with the data in Table 1.

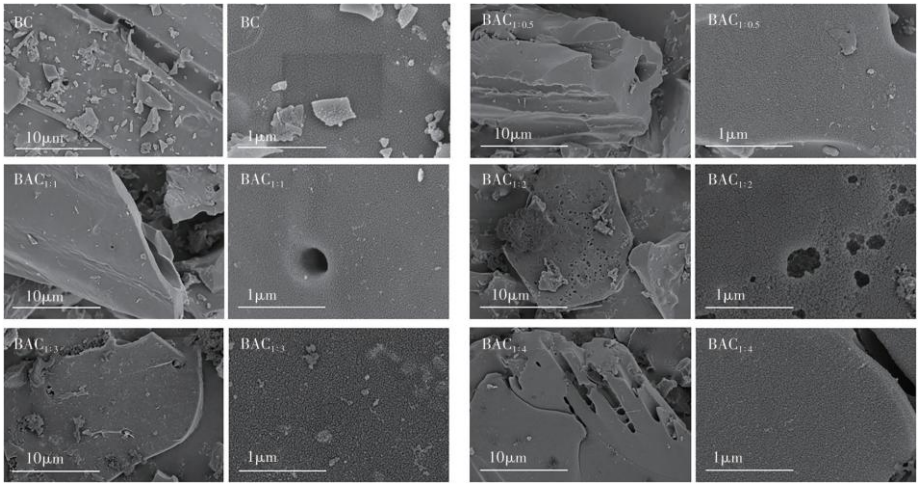

Figure 3 SEM images of bamboo charcoal (BC) and bamboo based activated carbon (BAC) with different BC/KOH mass ratios

Table 1 Specific surface area, total pore volume, and micropore volume of BACs

Sample	Specific surface area / ($m^2 \cdot g^{-1}$)	Total pore volume / ($cm^3 \cdot g^{-1}$)	Micropore volume / ($cm^3 \cdot g^{-1}$)
$BAC_{1:0.5}$	575	0.212	0.127
$BAC_{1:1}$	978	0.328	0.239
$BAC_{1:2}$	1395	0.421	0.341
$BAC_{1:3}$	1432	0.536	0.316
$BAC_{1:4}$	1286	0.465	0.259

3.1.2 Specific Surface Area and Pore Size Distribution of BAC

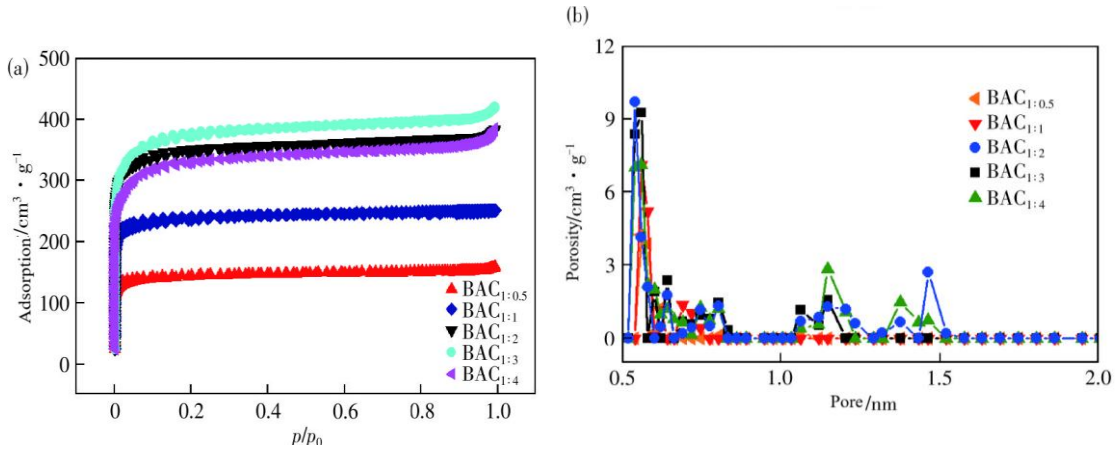

Figure 4 N2 adsorption desorption isotherms and pore size distribution of BAC

N_2 sorption isotherms for the BAC samples were acquired. The BET approach was employed for determining the specific surface area of BAC. while the pore size distribution was derived through NLDFT theoretical calculations. The outcomes are presented in Figure 4 and Table 1. Figure 4(a) reveals that the N_2 sorption profiles for all specimens conform to Type I isotherm characteristics. In the low-pressure region (relative

pressure <0.2), the N_2 adsorption amount of BAC increases rapidly, indicating the presence of a certain amount of micropores (pore size <1 nm) in BAC. Among them, $BAC_{1:2}$ and $BAC_{1:3}$ have the highest low-pressure N_2 adsorption capacity, while $BAC_{1:0.5}$ has the lowest, indicating that the micropore volume of $BAC_{1:2}$ and $BAC_{1:3}$ is significantly larger than that of $BAC_{1:0.5}$. At medium to high pressures, no significant increase in adsorption capacity was observed for all samples, indicating the absence of mesoporous and macroporous structures in the five BAC samples. As evidenced by Figure 4(b) and Table 1, an elevation in the KOH-to-BC mass ratio correlates with, an initial augmentation followed by a subsequent decline in both the specific surface area and total pore volume of BAC. The $BAC_{1:2}$ specimen demonstrates the optimal pore volume within the sub-1.0 nm pore size regime, whereas the specific surface area and cumulative pore volume attain their peak values at the $BAC_{1:3}$ composition.The above phenomenon can be explained as follows: due to the gradually enhanced erosion effect of the KOH activation process on the BC surface, the erosion effect becomes more significant as the KOH ratio increases. When the BC/KOH mass ratio reaches 1:2 and 1:3, $BAC_{1:2}$ and $BAC_{1:3}$ exhibit excellent microporous structural characteristics. Among these, $BAC_{1:2}$ exhibits a more pronounced abundance of micropores with diameters below 1.0 nm, whereas $BAC_{1:3}$ displays a broader pore size distribution.

3.1.3 Thermogravimetric Analysis

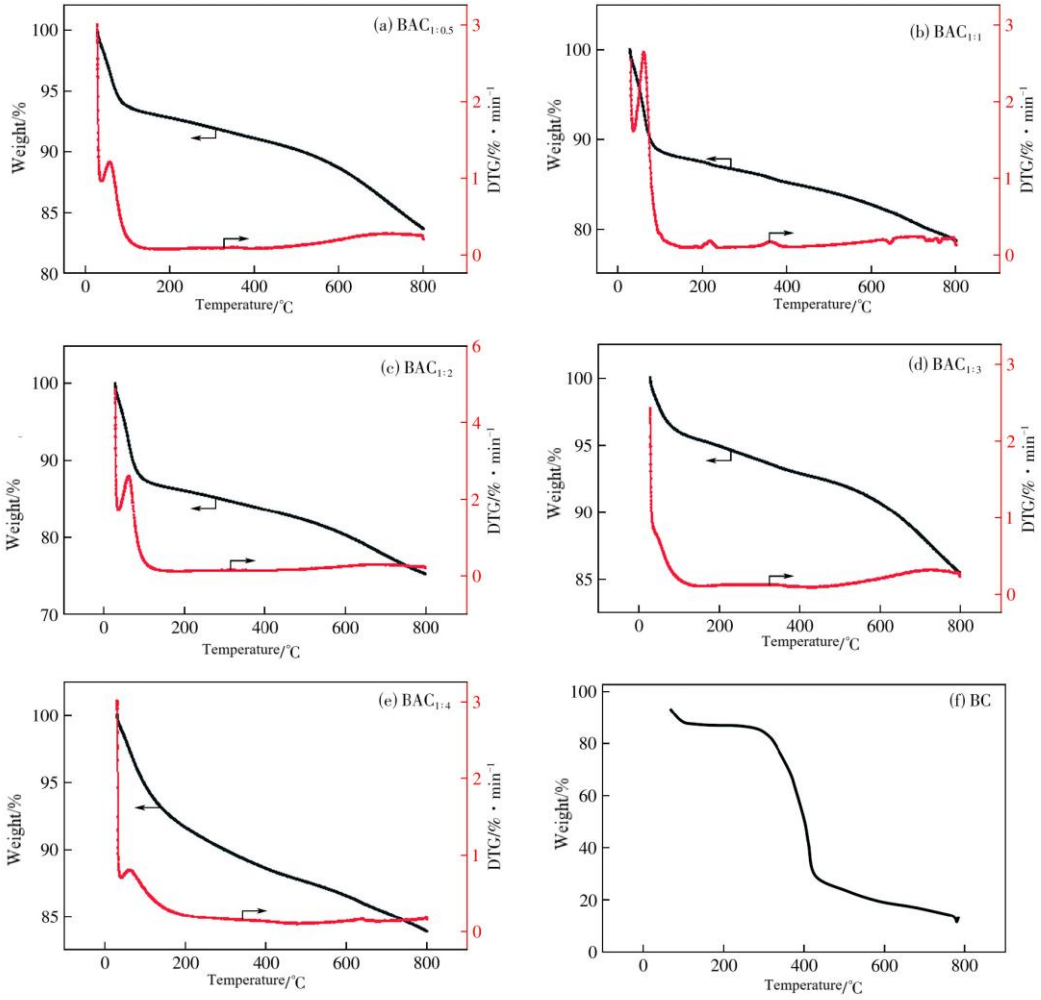

Figure 5 Thermogravimetric analysis of BAC and its activated precursor

Figure 5 shows the thermal stability characteristics of BAC and its precursor at 1073.2 K. TGA data not only characterize the carbon content of the precursor (a key parameter in activated carbon preparation) but also

reveal the stage characteristics of the material's thermal decomposition process: weight loss below 423.2 K (approximately 7%) originates from the desorption of free water in the material, while above 423.2 K, the carbonization-dominated stage begins. Since the research object is biomass material from the Gramineae family, its components include hemicellulose (thermal degradation onset temperature >427.2 K), cellulose (>523.2 K), and lignin (>553.2 K), and trace inorganic components also have a significant impact on mass loss during pyrolysis [35]. Specifically, the BC sample shows a significant mass decrease in the 553.2–798.2 K temperature range, a phenomenon resulting from the volatilization of organic components and the deconstruction of the biomass skeleton structure. In contrast, BAC does not exhibit obvious thermal sensitivity in the same temperature range, and its weight loss curve above 423.2 K corresponds only to the desorption process of adsorbed water. This difference indicates that the activation process effectively improves the thermal stability of the material, possibly by inhibiting high-temperature decomposition reactions through pore structure regulation and surface functional group modification.

3.2 Verification of Experimental Measurement Accuracy

Prior to quantifying the CO_2 capture capacity and kinetics in the hybrid formulation, the absorption performance of CO_2 in a baseline 30% DEA-H_2O solution at 313.2 K was initially evaluated to validate the experimental methodology. As depicted in Figure 6, the CO_2 uptake capacity determined for the 30% DEA-H_2O system in this investigation demonstrates strong concordance with previously published data, thereby confirming the reliability and validity of the experimental measurements employed herein [36].

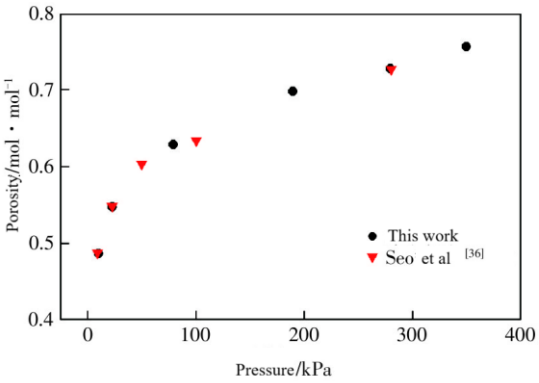

Figure 6 Absorption capacity of CO2 in 30% DEA-H2O (temperature 313.2K)

3.3 CO_2 Absorption (Adsorption) Rate in DEA-BAC-H_2O

3.3.1 Measurement of CO_2 Absorption (Adsorption) Rate

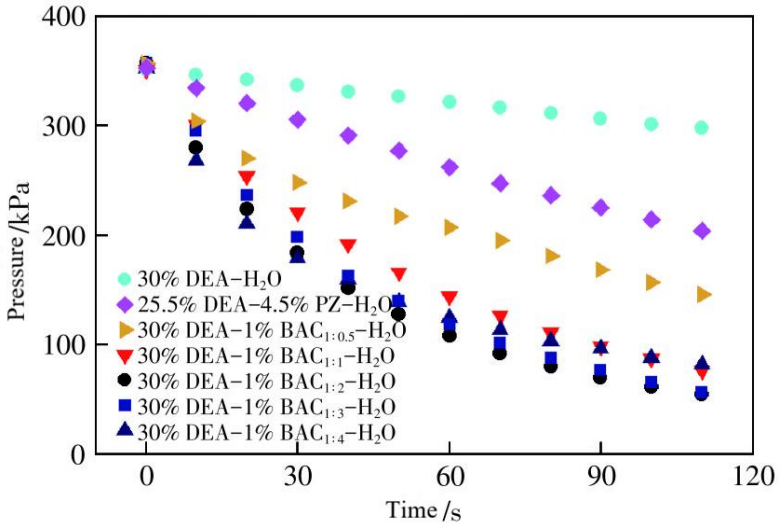

Figure 7 Absorption (adsorption) rate of CO2 in a mixed system

The CO_2 absorption (adsorption) rate in 30% DEA-1% BAC-H_2O (temperature 313.2 K) was measured and compared with the CO_2 absorption (adsorption) rates in 30% DEA-H_2O and 25.5% DEA-4.5% PZ-H_2O (commercial absorbent). The p-t curves of CO_2 in the six hybrid systems and 30% DEA-H_2O are shown in Figure 7. A faster drop in CO_2 partial pressure indicates a faster absorption (adsorption) rate. It can be seen that all five BAC samples with different activation ratios can significantly increase the CO_2 absorption (adsorption) rate in the DEA solution, and the CO_2 absorption (adsorption) rates are all higher than that of 25.5% DEA-4.5% PZ-H_2O. When the BC/KOH mass ratio increases to 1:2, the CO_2 absorption (adsorption) rate in 30% DEA-1% $BAC_{1:2}$-H_2O reaches the highest. Furthermore, the CO_2 absorption (adsorption) rates in the 30% DEA-1% BAC-H_2O systems containing $BAC_{1:3}$ and $BAC_{1:4}$ are similar, indicating that the pore size distributions of these BACs have analogous effects on the CO_2 absorption (adsorption) rate.

3.3.2 Apparent Absorption (Adsorption) Rate Constant

Employing Equation (3) in conjunction with the data presented in Figure 7, the apparent rate constants for CO_2 capture in 30% DEA-1% BAC-H_2O systems were determined. alongside those for 25.5% DEA-4.5% PZ-H_2O and 30% DEA-H_2O, were computed. To ensure the consistency of experimental results, measurement data from the first 120 seconds after the start of CO_2 absorption (adsorption) were used for rate constant calculation. As shown in Figure 8(a), ln[(n0−ne)/(n−ne)]exhibits a linear relationship with t, and kis the slope of this line. The kvalues of CO_2 in 30% DEA-1% BAC-H_2O, 25.5% DEA-4.5% PZ-H_2O, and 30% DEA-H_2O are shown in Figure 8(b). The kvalue of CO_2 in 30% DEA-1% $BAC_{1:2}$-H_2O is the highest, at $1.85\times10-2s^{-1}$. Meanwhile, the kvalues for the other hybrid systems containing $BAC_{1:0.5}$, $BAC_{1:1}$, $BAC_{1:3}$, and $BAC_{1:4}$ are $8.16\times10-3s^{-1}$, $1.52\times10-2s^{-1}$, $1.81\times10-2s^{-1}$, and $1.8\times10-2s^{-1}$, respectively. Furthermore, the kvalues of CO_2 in 25.5% DEA-4.5% PZ-H_2O and 30% DEA-H_2O are only $5.25\times10-3s^{-1}$ and $2.6\times10-3s^{-1}$, respectively. Therefore, the apparent CO_2 absorption (adsorption) rate constants of 30% DEA-1% BAC-H_2O are significantly increased compared to 30% DEA-H_2O. Specifically, the apparent absorption (adsorption) rate constant of CO_2 in 30% DEA-1% $BAC_{1:2}$-H_2O is 7 times and 3.5 times higher than those in 30% DEA-H_2O and 25.5% DEA-4.5% PZ-H_2O, respectively.

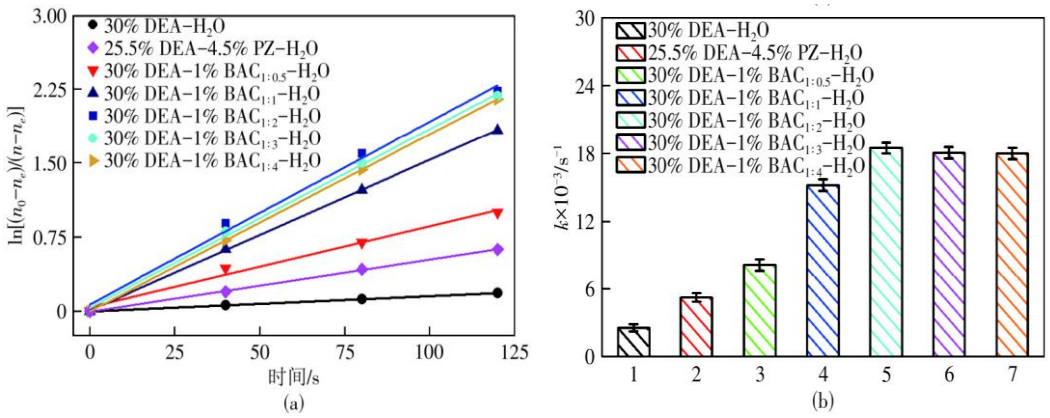

Figure 8 Calculation and numerical analysis of absorption (adsorption) rate constants of CO2 in a mixed system

To further investigate the effect of BAC addition amount on the apparent absorption (adsorption) rate constant, Figure 9 shows the changes in kvalues of the 30% DEA-BAC-H_2O system with different BAC addition amounts (0.5%, 1%, and 2%). Under the same BAC addition amount, as the BC/KOH mass ratio decreases, the kvalue of CO_2 in the 30% DEA-BAC-H_2O system first increases and then decreases. This occurrence may be rationalized by the divergent porous architectures of BAC arising from variations in the BC/KOH mass ratio. When the BC/KOH mass ratio is 1:2, the kvalue of CO_2 in the 30% DEA-BAC-H_2O system reaches the highest, which can be attributed to BAC_1:$_2$ having an appropriate specific surface area and the highest micropore volume (pore size less than 1.0 nm) [23]. Further comparing the curves for different BAC addition amounts reveals that when the BAC addition amount increases from 0.5% to 1%, the apparent CO_2 absorption (adsorption) rate constant increases significantly. However, when the BAC addition amount increases from 1% to 2%, the CO_2 absorption (adsorption) rate constant decreases noticeably. For example, in the 30% DEA-1% BAC_1:$_2$-H_2O system, when the BAC_1:$_2$ addition amounts are 0.5%, 1%, and 2%, the kvalues are 9.5×10−3s^{-1}, 1.85×10−2s^{-1}, and 1.0×10−2s^{-1}, respectively. The above phenomenon can be attributed to the different mechanisms of action caused by different solid content. When the BAC addition amount is low (mass fraction ≤1%), the introduction of BAC significantly enhances the CO_2 diffusion rate. That is, BAC adsorbs gas in the high-concentration CO_2 region and desorbs it into the liquid bulk in the low-concentration region via a shuttle effect under the concentration gradient. This dynamic process significantly improves the CO_2 diffusion efficiency. Even at low BAC concentrations, its high specific surface area can effectively enhance the CO_2 diffusion process [37]. However, when the BAC addition amount exceeds 1%, the agglomeration effect of BAC becomes significant, thereby reducing the effective specific surface area and CO_2 diffusion rate, leading to a decrease in the CO_2 absorption (adsorption) rate [38]. Therefore, introducing an appropriate amount of BAC can effectively increase the CO_2 diffusion rate in the DEA system, but excessive BAC content may reduce the CO_2 absorption (adsorption) rate due to particle agglomeration.

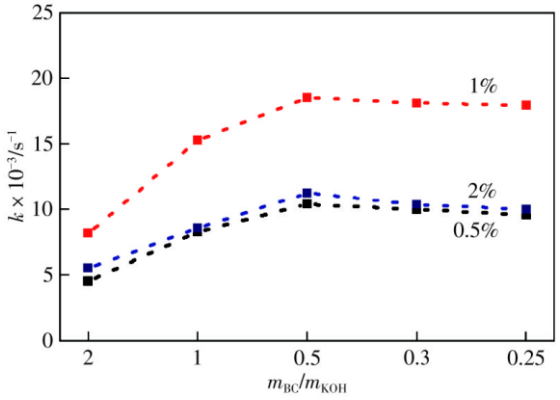

Figure 9 Apparent absorption (adsorption) rate constants of CO2 in 30% DEA-BAC-H2O system with different addition amounts

3.3.3 Analysis of Mass Transfer Resistance and Enhancement Mechanism of CO_2 in 30% DEA-1% BAC-H_2O

According to the analysis of mass transfer resistance using Equation (4), subtracting the reciprocal of the apparent absorption (adsorption) rate constant of each hybrid system from the mass transfer resistance of 30% DEA-H_2O and then dividing by the mass transfer resistance of 30% DEA-H_2O allows calculation of the reduction ratio of mass transfer resistance after introducing PZ or BAC into 30% DEA-H_2O, respectively. As shown in Figure 10, the mass transfer resistance of CO_2 in 30% DEA-1% BAC-H_2O is reduced by 68%–86% relative to 30% DEA-H_2O, significantly higher than the reduction ratio of 25.5% DEA-4.5% PZ-H_2O (42%). Simultaneously, the enhancement mechanism of introducing BAC differs from that of PZ; it does not introduce chemical action, meaning it will not lead to increased regeneration energy consumption. Consequently, the strategy of mitigating CO_2 diffusion limitations through the incorporation of bamboo-derived activated carbon surpasses the efficacy of conventional chemical promoter addition. This observation substantiates the hypothesis that diffusional resistance constitutes the primary kinetic bottleneck governing CO_2 absorption within DEA-based systems.

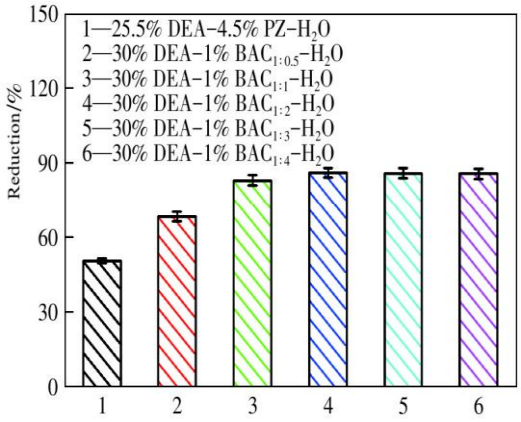

Figure 10 Reduction ratio of mass transfer resistance in the mixed system

The observed acceleration of CO_2 capture kinetics in DEA-H_2O systems upon BAC addition primarily originates from the catalytic influence of activated carbon on interfacial mass transport phenomena. Prior investigations have demonstrated that suspended solid particulates can facilitate CO_2 capture via the shuttle mechanism and interfacial boundary layer disruption. The shuttle effect posits that after activated carbon adsorbs CO_2, it releases it into the liquid phase under the concentration gradient, achieving cyclic transport between gas and liquid. The strong adsorption of gas by particles reduces the CO_2 concentration at the liquid interface, maintaining a high concentration gradient, thereby increasing the CO_2 absorption rate [39]. The boundary layer mixing mechanism suggests that solid particles around bubbles disturb the diffusion boundary layer, disrupting its stable structure and reducing its thickness. Since a thinner boundary layer shortens the diffusion path and reduces mass transfer resistance, it promotes CO_2 entry into the liquid phase and increases the mass transfer rate [40]. In conclusion, the incorporation of BAC substantially enhances the CO_2 capture performance of DEA-H_2O systems through the promotion of interfacial mass transfer between the gaseous and liquid phases. This provides an important basis for optimizing mass transfer enhancement strategies for amine-based absorbents.

3.4 Thermodynamics of CO_2 Absorption (Adsorption) in 30% DEA-BAC$_{1:2}$-H_2O

3.4.1 CO_2 Absorption (Adsorption) Capacity in 30% DEA-BAC$_{1:2}$-H_2O

Within the pressure range of 0–0.35 MPa at 313.2 K, the CO_2 absorption (adsorption) capacities in 30% DEA-BAC_1:$_2$-H_2O with different BAC_1:$_2$ addition amounts (0, 0.5%, 1%, 2%) were measured. As shown in Figure 11(a), the CO_2 absorption (adsorption) capacity increases with rising CO_2 partial pressure, showing a trend of first rising and then leveling off, reflecting the chemical absorption characteristics of this system. Simultaneously, as the mass fraction of BAC_1:$_2$ increases, the CO_2 absorption (adsorption) capacity shows a decreasing trend. When the BAC_1:$_2$ addition amount is 0.5%, its CO_2 absorption (adsorption) capacity decreases from 2.15 mol/kg to 2.02 mol/kg, a reduction of approximately 6.1%. Furthermore, when the mass fraction of BAC_1:$_2$ increases to 1% and 2%, the CO_2 absorption (adsorption) capacity decreases by 7% and 12%, respectively. Therefore, compared to the chemical absorption of CO_2 by DEA, the introduction of BAC_1:$_2$ does not increase the CO_2 absorption capacity of the DEA solution. On the other hand, BAC has a developed microporous and mesoporous structure, which easily adsorbs organic amine molecules, thereby reducing the effective concentration of free amine in 30% DEA-BAC_1:$_2$-H_2O and weakening the chemical absorption capacity of CO_2 by DEA [41].

Continuing to use the 30% DEA-1% BAC_1:$_2$-H_2O hybrid system as the research object, the CO_2 absorption (adsorption) capacities within the pressure range of 0–0.35 MPa were systematically measured at three temperatures: 313.2 K, 333.2 K, and 353.2 K, as shown in Figure 11(b). Experimental data show that the CO_2 absorption (adsorption) capacity of this system decreases stepwise with increasing temperature: the capacity decreases by 7.5% in the 313.2–333.2 K temperature range, and the decrease expands to 19.5% when the temperature rises to 353.2 K. Notably, at the high temperature of 353.2 K, the system still maintains an effective capacity above 1.6 mol/kg, confirming its good adaptability to high-temperature operating conditions.

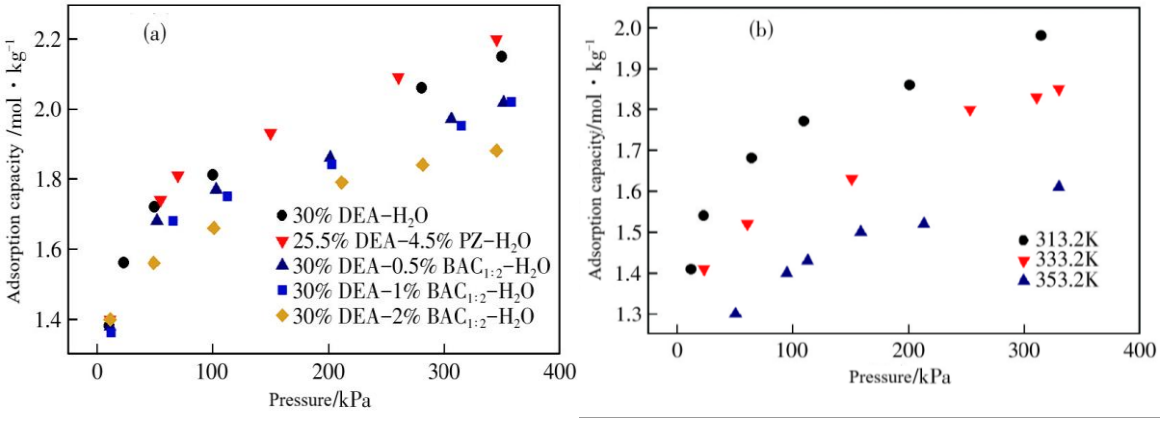

Figure 11 Absorption (adsorption) capacity of CO2 at different solid contents and temperatures in 30% DEA-BAC1:2-H2O

3.4.2 CO_2 Desorption Enthalpy in 30% DEA-1% BAC_1:$_2$-H_2O

Based on Equation (5) and Figure 11(b), the CO_2 desorption enthalpies in 30% DEA-1% BAC_1:$_2$-H_2O, 25.5% DEA-4.5% PZ-H_2O, and 30% DEA-H_2O (313.2 K) were calculated. As shown in Figure 12, the CO_2 desorption enthalpies in 30% DEA-H_2O, 30% DEA-1% BAC_1:$_2$-H_2O, and 25.5% DEA-4.5% PZ-H_2O are 75 kJ/mol, 60 kJ/mol, and 80 kJ/mol, respectively. Therefore, compared to 30% DEA-H_2O and 25.5% DEA-4.5% PZ-H_2O, the CO_2 desorption enthalpy in 30% DEA-1% BAC_1:$_2$-H_2O is reduced by 20% and 25%, respectively, indicating that the introduction of BAC_1:$_2$ facilitates the CO_2 desorption process.

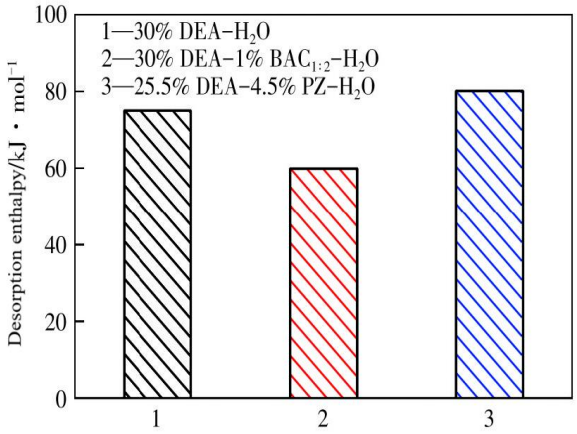

Figure 12 Desorption enthalpy of CO2 in different BAC addition levels of 30% DEA-1% BAC1:2-H2O

3.5 Cycling Regeneration Performance of 30% DEA-1% BAC_1:$_2$-H_2O

The regenerative stability of the hybrid system under cyclic operation represents another critical determinant for its industrial viability, as illustrated in Figure 13. After 5 cycles of use [absorption (adsorption) at 313.2 K and regeneration at 373.2 K], the CO_2 absorption (adsorption) capacity of 30% DEA-1% BAC_1:$_2$-H_2O decreased from the initial 0.088 g/g to 0.072 g/g, with a capacity decay rate of approximately 18.2%, showing relatively high cycling stability. This performance decay may originate from the slight volatilization of amine solution or the generation of thermal degradation by-products during high-temperature regeneration. Compared to the typical data of conventional organic amines (such as MEA) with a cycling capacity decrease of 25%–30%, the decay rate of this system is significantly lower, indicating relatively stable CO_2 absorption (adsorption) capacity. The experimental findings indicate that the 30% DEA-1% BAC_1:$_2$-H_2O formulation exhibits promising potential for sustained industrial deployment.Overall, the developed 30% DEA-BAC_1:$_2$-H_2O hybrid system is significantly superior to 30% DEA-H_2O and 25.5% DEA-4.5% PZ-H_2O in terms of CO_2 absorption (adsorption) rate, while also having a lower CO_2 desorption enthalpy. Furthermore, the decrease in CO_2 absorption (adsorption) capacity is not significant. However, the following key issues need to be addressed in future research: 1) Detailed process simulation is required, along with pilot-scale experiments on CO_2 absorption (adsorption) in 30% DEA-1% BAC_1:$_2$-H_2O and studies on the long-term stability and degradation characteristics of this system. 2) The microporous architecture and specific surface area of BAC warrant additional refinement to augment the carbon dioxide capture performance of the integrated system. Specialized absorption/desorption cycling apparatus compatible with solid-laden hybrid systems requires further engineering advancement to enhance mass transfer kinetics throughout the CO_2 capture operation. addressing the inherent challenge of non-uniform solid particle dispersion, thereby improving the scalability and commercial viability of this approach.

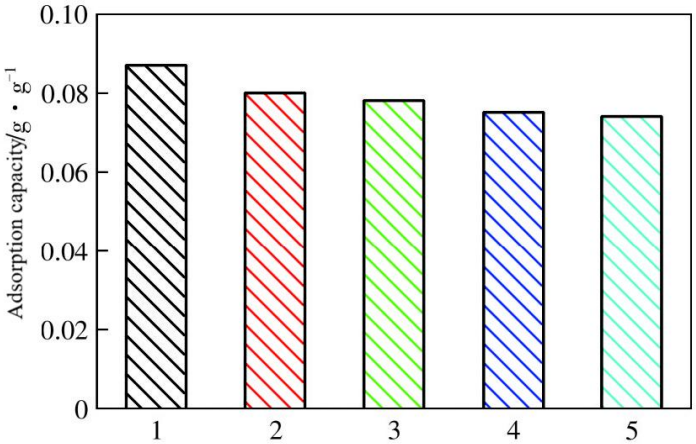

Figure 13 Cycle regeneration performance of 30% DEA-1% BAC1:2-H2O

4 Conclusion

(1) Five distinct bamboo-based activated carbon samples were fabricated by modulating the mass proportions of bamboo charcoal to potassium hydroxide. All have a high proportion of micropores and specific surface area. These bamboo-based activated carbons significantly increased the CO_2 absorption rate of 30% DEA-H_2O.

(2) The CO_2 absorption (adsorption) rate in 30% DEA-1% $BAC_{1:2}$-H_2O is 7 times and 3.5 times that in 30% DEA-H_2O and 25.5% DEA-4.5% PZ-H_2O (commercial absorbent), respectively.

(3) The CO_2 desorption enthalpy in this system decreased by 20% and 25% compared to 30% DEA-H_2O and 25.5% DEA-4.5% PZ-H_2O, respectively, and the CO_2 absorption (adsorption) capacity is moderate. Furthermore, 30% DEA-1% $BAC_{1:2}$-H_2O shows good cycling regeneration performance.

References

[1] XIAO Yurou Celine, SUN Siyu Sonia, ZHAO Yong, et al. Reactive capture of CO_2 via amino acid[J]. Nature Communications, 2021, 15(1): 7849.

[2] LEE Geonhui, LI Yuguang C, KIM Ji-Yong, et al. Electrochemical upgrade of CO_2 from amine capture solution[J]. Nature Energy, 2021, 6(1): 46-53.

[3] JABRAEELZADEH Ali, GHAREHGHANI Ayat, AHBABI SARAY Jabraeil, et al. Techno-economic analysis of biogas upgrading through amine scrubbing: A comparative study of different single amines[J]. Fuel, 2022, 381: 133662.

[4] MENG Fanzhi, MENG Yuan, JU Tongyao, et al. Research progress of aqueous amine solution for CO_2 capture: A review[J]. Renewable and Sustainable Energy Reviews, 2022, 168: 112902.

[5] SHOKROLLAHI F, LAU K K, PARTOON B, et al. A review on the selection criteria for slow and medium kinetic solvents used in CO_2 absorption for natural gas purification[J]. Journal of Natural Gas Science and Engineering, 2022, 98: 104390.

[6] SHARIF Maimoona, GE Chunliang, ZHANG Wei, et al. Molecular dynamics investigation of flue gas effects on CO_2 diffusion and absorption in water lean amine-based solvents[J]. Journal of Molecular Liquids, 2020, 419: 126732.

[7] DAS Bisweswar, GUO Haijun, XIONG Lian, et al. Piperazine-activated diethanolamine formulation for post-combustion CO_2 capture[J]. Journal of Industrial and Engineering Chemistry, 2023, 118: 519-532.

[8] XIAO Sini, LIU Helei, GAO Hongxia, et al. Kinetics and mechanism study of homogeneous reaction of CO_2 and blends of diethanolamine and monoethanolamine using the stopped-flow technique[J]. Chemical Engineering Journal, 2017, 316: 592-600.

[9] ZHAO Yujing, XIANG Sheng, DU Jian, et al. Computer-aided amine solvent design for carbon capture based on desorption thermodynamic and reaction kinetic models[J]. Separation and Purification Technology, 2015, 360: 130984.

[10] LU Xiaohua, CHEN Yifeng, DONG Yihui, et al. Nano-interface enhanced CO_2 absorption and mechanism analysis[J]. CIESC Journal, 2020, 71(1): 34-42. (in Chinese)

[11] WANG Bo, WANG Jinyu, CHEN Yuan, et al. The absorption behavior of SO_2 by amine alkyl organosilicon: Experimental analysis and numerical simulation[J]. Chemical Engineering Journal, 2023, 474: 145345.

[12] ALIVAND Masood S, MAZAHERI Omid, WU Yue, et al. Preparation of nanoporous carbonaceous promoters for enhanced CO_2 absorption in tertiary amines[J]. Engineering, 2020, 6(12): 1381-1394.

[13] WANG Zengding, ZHANG Tianjiang, LIU Shanchao, et al. Unveiling nanoscale fluid miscible behaviors with nanofluidic slim-tube[J]. Energy & Environmental Science, 2021, 17(24): 9635-9651.

[14] JIANG Jiaotong, ZHAO Bo, ZHUO Yuqun, et al. Experimental study of CO_2 absorption in aqueous MEA and MDEA solutions enhanced by nanoparticles[J]. International Journal of Greenhouse Gas Control, 2014, 29: 135-141.

[15] LIU Wei, ZHANG Min, ZHU Zhaoqi, et al. Preparation and current applications of black titanium dioxide nanomaterials[J]. Chemical Industry and Engineering Progress, 2020, 44(1): 341-353.

[16] WEN Chang, LIU Tianyu, WANG Dapeng, et al. Biochar as the effective adsorbent to combustion gaseous pollutants: Preparation, activation, functionalization and the adsorption mechanisms[J]. Progress in Energy and Combustion Science, 2023, 99: 101098.
[17] VALLACE Anthony, REN Yi, JONES Christopher W, et al. Kinetic model describing self-limiting CO_2 diffusion in supported amine adsorbents[J]. Chemical Engineering Journal, 2023, 472: 144838.
[18] TEIMOURI Zahra, NANDA Sonil, ABATZOGLOU Nicolas, et al. Application of activated carbon in renewable energy conversion and storage systems: A review[J]. Environmental Chemistry Letters, 2023, 22(3): 1073-1092.
[19] CHANDOLIYA Rakhi, SHARMA Shivika, SHARMA Vikas, et al. Titanium dioxide nanoparticles: A comprehensive review on synthesis, applications and toxicity[J]. Plants, 2023, 13(21): 2964.
[20] SINGH Gurwinder, LEE Jangmee, KARAKOTI Ajay, et al. Emerging trends in porous materials for CO_2 capture and conversion[J]. Chemical Society Reviews, 2020, 49(13): 4360-4404.
[21] UMAR Mustapha, YUSUF Basiru O, ALIYU Mansur, et al. Advancing frontiers in CO_2 capture: The renaissance of biomass-derived carbon materials[J]. Coordination Chemistry Reviews, 2020, 526: 216380.
[22] LU Sumin, XING Min, SUN Yan, et al. Experimental and theoretical studies of CO_2 absorption enhancement by nano-Al_2O_3 and carbon nanotube particles[J]. Chinese Journal of Chemical Engineering, 2013, 21(9): 983-990.
[23] CHEN Yifeng, LI Bei, WANG Ao, et al. Developing aqueous porous carbons for biogas upgrading[J]. Separation and Purification Technology, 2020, 329: 125146.
[24] KHOSHRAFTAR Zohreh, GHAEMI Ahad. Presence of activated carbon particles from waste walnut shell as a biosorbent in monoethanolamine (MEA) solution to enhance carbon dioxide absorption[J]. Heliyon, 2022, 8(1): e08689.
[25] VALI Indudhar Panduranga, ANUSHA B. S, PRUTHVIJA M, et al. Bamboo and coconut shell based activated carbon: A Raman spectroscopic study[J]. Materials Chemistry and Physics, 2023, 318: 129240.
[26] CHEN Siming, ZHANG Sichao, GAO Huailing, et al. Mechanically robust bamboo node and its hierarchically fibrous structural design[J]. National Science Review, 2023, 10(2): nwac195.
[27] HEO Sujeong, KIM Wooram, JO Youngmin, et al. Fabrication of bamboo-based activated carbon for low-level CO_2 adsorption toward sustainable indoor air[J]. Sustainability, 2023, 16(4): 1634.
[28] WEI Haoran, DENG Shubo, HU Bingyin, et al. Granular bamboo-derived activated carbon for high CO_2 adsorption: The dominant role of narrow micropores[J]. ChemSusChem, 2012, 5(12): 2354-2360.
[29] CHEN Yifeng, YIN Haoran, WEN Shitao, et al. Biogas upgrading using aqueous bamboo-derived activated carbons[J]. Bioresource Technology, 2015, 419: 132055.
[30] BAG Oznur, TEKIN Kubilay, KARAGOZ Selhan. Microporous activated carbons from lignocellulosic biomass by KOH activation[J]. Fullerenes, Nanotubes and Carbon Nanostructures, 2020, 28(12): 1030-1037.
[31] XU Qingqiang, YIN Haoran, ZHOU Dong, et al. Kinetic study on the promotion of CO_2 absorption in aqueous N-methyldiethanolamine by amino-functionalized ionic liquids[J]. Separation and Purification Technology, 2019, 362: 131707.
[32] CHEN Yifeng, LI Biao, WU Jian, et al. Kinetics study and performance comparison of CO_2 separation using aqueous choline-amino acid solutions[J]. Separation and Purification Technology, 2021, 261: 118284.
[33] TIWARI Surya Chandra, PANT Kamal Kishore, UPADHYAYULA Sreedevi. Kinetics study and modeling of CO_2 capture in new class dual-functionalized ionic liquid blend methyl diethanolamine absorbents[J]. Industrial & Engineering Chemistry Research, 2022, 63(17): 7578-7592.
[34] NGUYEN William Hoang Chi Hieu, HENNI Amr. Performance of a high capacity polyamine: Measurement and modeling of the solubility of carbon dioxide in aqueous solutions of 1,4-bis(3-aminopropyl)piperazine and its heat of absorption[J]. Journal of Environmental Chemical Engineering, 2023, 11(5): 110431.
[35] PLAZA M G, PEVIDA C, ARIAS B, et al. Different approaches for the development of low-cost CO_2 adsorbents[J]. Journal of Environmental Engineering, 2009, 135(6): 426-432.
[36] SEO Dong-Joo, HONG Won-Hi. Solubilities of carbon dioxide in aqueous mixtures of diethanolamine and 2-amino-2-methyl-1-propanol[J]. Journal of Chemical & Engineering Data, 1996, 41(2): 258-260.
[37] LI He. CO_2 capture by various nanoparticles: Recent development and prospective[J]. Journal of Cleaner Production, 2023, 414: 137679.
[38] LEE Wonhyeok, XU Ronghuan, KIM Seonggon, et al. Nanofluid and nanoemulsion absorbents for the enhancement of CO_2 absorption performance[J]. Journal of Cleaner Production, 2021, 291: 125848.
[39] LOU Baohui, WU Xianhao, ZHANG Chi, et al. Advances in nanofluid for CO_2 absorption and separation[J]. Chemical Industry and Engineering Progress, 2023, 42(7): 3802-3815.

[40] YUAN Cuiting, WANG Yan, BAENA-MORENO Francisco M, et al. Review and perspectives of CO_2 absorption by water- and amine-based nanofluids[J]. Energy & Fuels, 2023, 37(13): 8883-8901.
[41] MENDONCA Thais Aline Prado, NASCIMENTO Joao Paulo C, CASAGRANDE Gleison Antonia, et al. Ethylenediamine-modified activated carbon photocatalyst with the highest TiO_2 attachment dispersion for improved photodegradation of sulfamethazine[J]. Materials Chemistry and Physics, 2022, 318: 129203.
[42] NARCISO Claudia Rosa Hernández, MARTINEZ Cristina G, O'CONNELL Brendan, et al. Thermophysical behavior of carbonated aqueous solutions containing monoethanolamine and degradation products[J]. Journal of Chemical & Engineering Data, 2022, 69(10): 3435-3449.